Available online at www.sciencedirect.com
ScienceDirect
Thermochimica Acta 448 (2006) 1–6
thermochimica acta
www.elsevier.com/locate/tca

Solid-state kinetics of thermal release of pyridine and morphological study of $[Ni(ampy)_2(NO_3)_2]$; ampy = 2-picolylamine

Sumanta Kumar Padhi *

Department of Chemistry, Indian Institute of Technology Guwahati, Guwahati 781039, Assam, India

Received 24 April 2006; received in revised form 19 June 2006; accepted 21 June 2006
Available online 27 June 2006

Abstract

The re-examined X-ray crystal structure of $[Ni(ampy)_2(NO_3)_2]$; ampy = 2-picolylamine belongs to monoclinic $P2_1/c$ space group having, $a = 8.73510(10)$ Å, $b = 8.73690(10)$ Å, $c = 10.26480(10)$ Å and $\beta = 101.5610(10)^\circ$. The microscopic feature calcined at 600 °C displays a thread type fiber of NiO. The thermogravimetric analysis shows that the thermal decomposition occurs in three steps where the removal of ligand occurs in an exothermic process. The activation energy was estimated with both iso-conversional and multivariate non-linear-regression methods. Friedman method agrees with a first-order kinetics having activation energy E and logarithmic pre-exponential factor A, 41 ± 1 kJ mol^{-1} and 2.54, respectively. Multivariate non-linear-regression methods show expanded Prout–Tompkins Bna model is the best fit model with highest correlation coefficient 0.999998 followed by Cn which corresponds to the nth order reaction with auto catalysis through the reactants. The calculated apparent activation energies are consistent with iso-conversional methods. The corresponding function $f(\alpha)$, activation energy E and logarithmic pre-exponential factor A of Bna model, are $(1-\alpha)^{2.08}\alpha^{1.0236E-3}$, 42 kJ mol^{-1}and 3.12, respectively, and those of Cn model are $(1-\alpha)^{2.07}(1+0.0144\alpha)$, 42 kJ mol^{-1} and 3.11, respectively. The calculated rate constant and half-life time from iso-concentration plot are 2.381×10^{-3} s^{-1} and 291 s, respectively.

Keywords: 2-Picolylamine complex of nickel(II)nitrate; X-ray crystallography; Morphology of the complex; Kinetics of thermal decomposition; Iso-conversional method; Multivariate non-linear-regression

1. Introduction

The design and synthesis of nickel(II)ampy complexes, has been extensively studied over past few decades [1–3]. The utility of such complexes as molecule-based magnets and photomagnetic properties are widely reported. The presence of ferromagnetic and antiferromagnetic interactions in 1D, 2D and 3D bimetallic complexes obtained through self-assembly processes having $M^{2+/3+}$–Ni^{2+} pairs are the exciting one in modern chemistry [1]. Magnetic phase transitions at lower temperatures in different molecular architecture of such molecules are most impulsive.

This application oriented field stems our interest through a close look towards the thermal decomposition of $[Ni(ampy)_2(NO_3)_2]$ at static nitrogen atmosphere. In this article we report the thermal and morphological study of $[Ni(ampy)_2(NO_3)_2]$. Iso-conversional, Non-isothermal and iso-thermal methods are being widely studied here. Combination of both iso-conversional and multivariate non-linear-regression can provide most reasonable models than the model-fitting methods.

2. Experimental

2.1. Materials

$[Ni(ampy)_2(NO_3)_2]$; (ampy = 2-picolylamine) was synthesized by the reported procedure [1]. An ORTEP (30% probability) diagram is shown in Fig. 1 [4]. Nickel(II)nitrate hexahydrate was purchased from Merck India Ltd. 2-Picolylamine was purchased from M/S Aldrich, USA. All the chemicals and solvents (reagent grade) were used as received without further purifications.

2.2. Instrumentation and methods

FT-IR spectra of range 4000–400 cm^{-1} were recorded using Perkin-Elmer Spectrum One in KBr disc. SEM studies were

* Tel.: +91 361 2582345; fax: +91 361 2690762.
E-mail address: sumanta@iitg.ernet.in.

0040-6031/$ – see front matter © 2006 Published by Elsevier B.V.
doi:10.1016/j.tca.2006.06.015

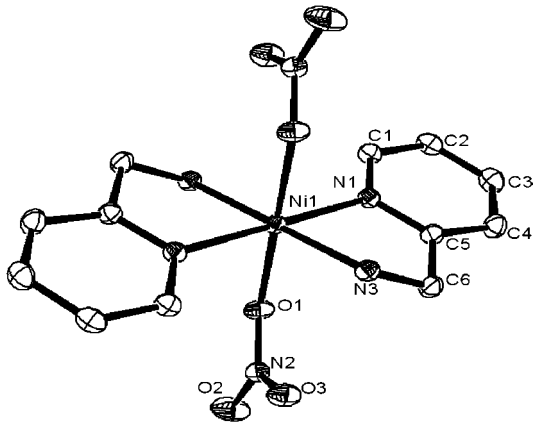

Fig. 1. ORTEP (30% probability) of $[Ni(ampy)_2(NO_3)_2]$.

done by Variable Pressure Digital Scanning Electron Microscope (model LEO 1430 VP) with EDS for X-ray Microanalysis.

2.2.1. X-ray crystallography

Single crystals X-ray crystallographic data were collected using Bruker SMART APEX-CCD diffractometer with Mo Kα radiation (λ = 0.71073 Å). The intensity data were corrected for Lorentz and polarization effects and empirical absorption corrections was applied using SAINT program [5]. The structure was solved by direct methods using SHELXS-97 and non-hydrogen atoms located from the difference Fourier maps were refined anisotropically by full-matrix least-squares on F^2 using SHELXL-97 [6]. The hydrogen atoms were included in the calculated positions and refined isotropically using a riding model. Table 1 shows the crystal data and parameters.

Table 1
Crystal data and refinement

Formula	$C_{12}H_{16}N_6O_6Ni$
M_r	394.99
Crystal color, habit	Blue, blocks
T (K)	296 (2)
Wave length (Å)	0.71073
Crystal system	Monoclinic
Space group	$P2_1/c$
a (Å)	8.73510 (10)
b (Å)	8.73690 (10)
c (Å)	10.26480 (10)
β (°)	101.5610 (10)
V (Å^3)	767.492 (15)
Z	2
$F(0\,0\,0)$	404
ρ_{calc} (g cm^{-3})	1.709
μ (mm^{-1})	1.310
GOF on F^2[a]	1.068
R_1[b] (%)	2.03
wR_2[c] (%)	5.88

[a] $\mathrm{GOF} = [\sum[w(F_0^2 - F_c^2)^2]/M - N]^{1/2}$ (M = number of reflections, N = number of parameters refined).
[b] $R_1 = \sum ||F_0| - |F_c||/\sum |F_0|$.
[c] $wR_2 = [\sum[w(F_0^2 - F_c^2)^2]/\sum[w(F_0^2)^2]]$.

2.2.2. Thermogravimetry (TG) measurements

The thermal behaviors including thermal decomposition temperature were determined by a computer controlled METTLER TOLEDO STAR[e] system of module TGA/SDTA851[e] under static nitrogen atmosphere. Prior to record the data the instrument was properly calibrated and sensor used here is RTypS-DTA. Decompositions were recorded for the sample upon platinum pan. Onset temperature of DTG curve used to evaluate the onset decomposition temperature, which estimates the thermal stability of the sample. TG data were recorded at a heating rate of 10 °C min^{-1} from 25 to 700 °C under static nitrogen atmosphere.

2.2.3. Differential scanning calorimetry (DSC) measurements

The thermal behaviors were studied by a computer controlled METTLER TOLEDO STAR[e] system of module DSC821[e] under static nitrogen atmosphere. Prior to recording the data, the temperature and energy of the instrument were calibrated with standard indium and ceramic sensor FRS5. A 70 μL aluminum reference pan was used and the data were recorded from 25 to 600 °C at heating rates of 5, 10, 15, 20 and 25 °C min^{-1}.

2.2.4. Methods

Iso-conversional methods and Multivariate non-linear-regression methods were performed by Netzsch TA4 thermokinetics software.

3. Results and discussion

3.1. Proposed mechanism of thermal decomposition

3.1.1. FT-IR and morphological study

The FT-IR spectra (Fig. 2), shows both $\nu(NH_2)_{as}$ and $\nu(NH_2)_s$ which is present at 3341 and 3288 cm^{-1} vanishes with the increase of temperature [7,8]. The aromatic region at 1610 cm^{-1} gradually becomes absent from the original peak after 280 °C. At 340 °C, the removal of pyridine is not completed as it shows the presence of aromatic peak at 1596 cm^{-1}. At 600 °C $\nu(Ni–O)_{str}$ appears at 531 cm^{-1}.

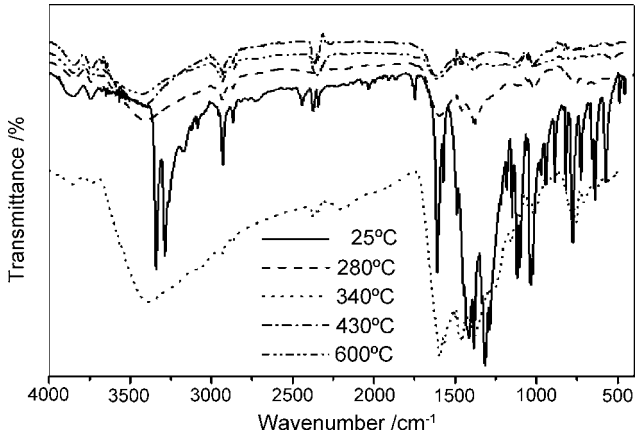

Fig. 2. FT-IR spectra observed at different temperatures for $[Ni(ampy)_2(NO_3)_2]$.

The morphological evolution of powdered [Ni(ampy)$_2$(NO$_3$)$_2$] was examined by SEM (Fig. 3) after calcinations. At 280 °C (Fig. 3A) the microscopic feature shows a porous metallic surface resulting from the elimination of $NO_{(g)}$. A jelly type fiber started to form (Fig. 3B) at 340 °C where pyridine gets sublimed, contains 2.16% (by weight) N-content in the composition. Complete removal of pyridine at 430 °C shows a layered fiber (Fig. 3C). In (Fig. 3D) the morphological view shows thread type fibers of NiO.

3.1.2. Thermal decomposition

The TG, DTG curves in Fig. 4 displays the weight loss in three distinct steps. Removal of two moles of $NO_{(g)}$ (15.09%, *ca.* 15.18%) occurs in step I at DTG midpoint 217 °C within the temperature range 154–285 °C. In step II two moles of pyridine (40.63%, *ca.* 40.05%) gets removed at DTG midpoint 309 °C within the temperature range 285–345 °C. Step III shows the formation of volatile components leaving behind one mole of NiO (19.11%, *ca.* 18.91%) as residual part at 588 °C. The thermal decompositions are provided in the following equations:

- Step I $[Ni(ampy)_2(NO_3)_2] \xrightarrow{\Delta} 2NO \uparrow + Residue\,(R)$
- Step II $R \xrightarrow{\Delta} 2Py + Residue\,(R_1)$
- Step III $R_1 \xrightarrow{\Delta} Product_{(volatile)} + NiO(s)$

The DSC curve (Fig. 5) indicates that the removal of both $NO_{(g)}$ and 2-picolylamine occurs through exothermic processes in the range of 180–375 °C. The fractional DSC profile begins with an endothermic up to 150 °C and irreversible exothermic ending.

3.2. Kinetics of thermal decomposition

3.2.1. Iso-conversional methods

In iso-conversional method it is assumed that a degree of conversion α can be explicitly assigned to each point of the reaction curve. The kinetic analysis was considered for the elimination of pyridine in Step II, taking into account the DSC curves within temperature span 285–345 °C, utilizing Friedman and ASTM E698 methods [9–16].

3.2.1.1. Friedman method. The convergence of the activation energy values obtained by means of a differential method like the Friedman method with those resulting from using integral methods with integration over small ranges of reaction progress α, comes from the fundamentals of the differential and integral calculus [9–14]. Friedman analysis follows the mathematical equation:

$$\ln(d\alpha/dt)|_{\alpha-\alpha_j} = \ln A - \frac{E}{RT_{kj}} + \ln f(\alpha_j)$$

where E is the activation energy, A the pre-exponential factor; R corresponds to universal gas constant. The kinetic parameters were extracted from the experimental enthalpy change data using

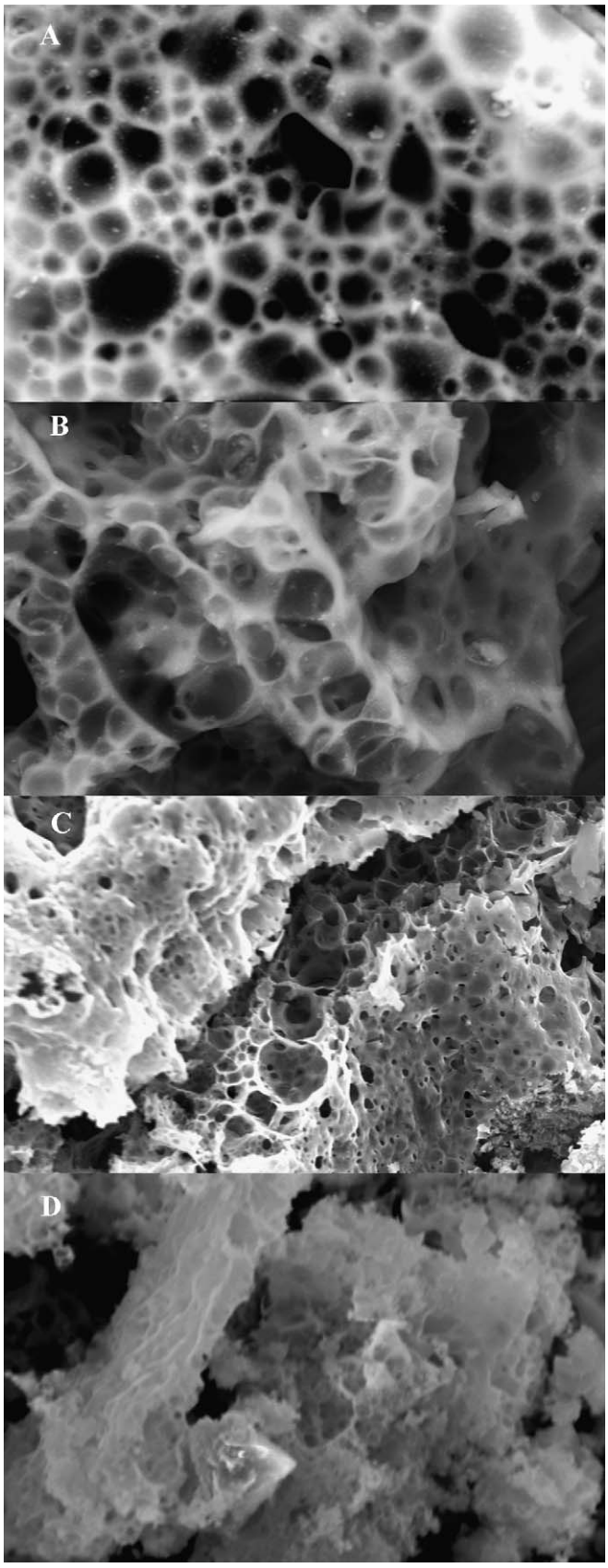

Fig. 3. SEM morphological aspects for [Ni(ampy)$_2$(NO$_3$)$_2$] calcined at: (A) 280 °C, (B) 340 °C, (C) 430 °C and (D) 600 °C.

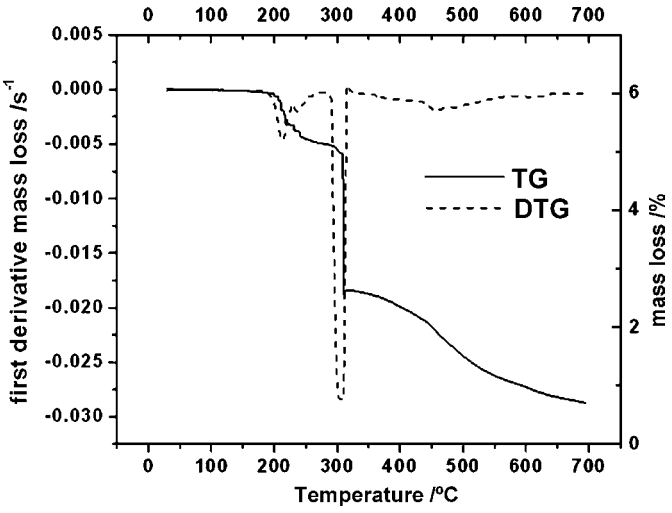

Fig. 4. TG/DTG plot of $[Ni(ampy)_2(NO_3)_2]$ at a heating rate 10 °C min^{-1}.

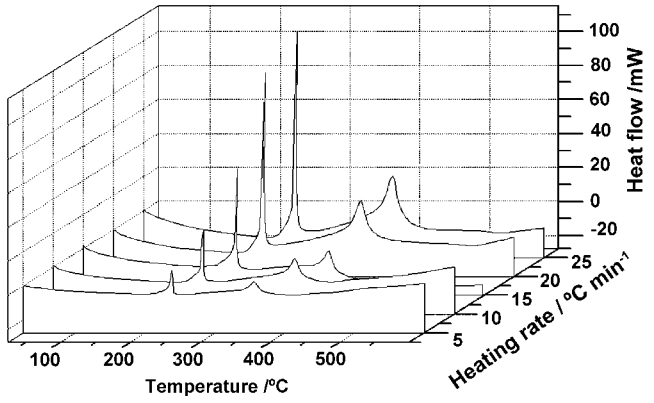

Fig. 5. DSC curves at heating rates 5–25 °C min^{-1}.

following transformation (Table 2):

$$\alpha = \frac{\Delta H_{\text{part}}}{\Delta H_{\text{tot}}}$$

Table 2
Arrhenius parameters in Friedman analysis

α	Friedman analysis	
	E (kJ mol^{-1})	log A (s^{-1})
0.02	43.13 ± 0.04	3.27
0.05	42.20 ± 0.09	3.08
0.10	42.37 ± 0.07	3.09
0.20	42.37 ± 0.10	3.03
0.30	42.38 ± 0.08	2.97
0.40	42.40 ± 0.01	2.90
0.50	42.43 ± 0.10	2.82
0.60	42.46 ± 0.07	2.71
0.70	42.52 ± 0.08	2.59
0.80	42.67 ± 0.10	2.41
0.90	43.37 ± 0.28	2.16
0.95	45.20 ± 0.13	2.00
0.98	24.82 ± 0.68	0.00
Average	41.41 ± 0.14	2.54

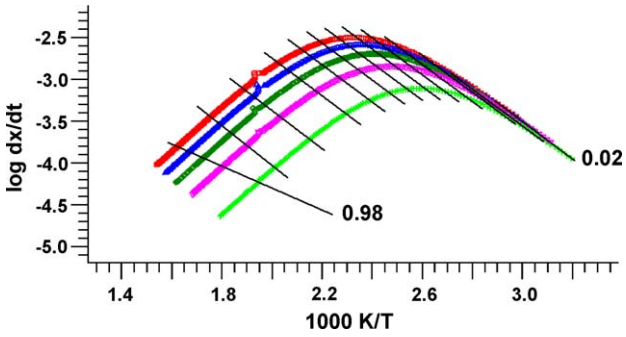

Fig. 6. Logarithmic rate as function of reciprocal of temperature by Friedman method.

where α is the general variable reaction degree, ΔH_{part} the partial area (J g^{-1}), and ΔH_{tot} is the total peak area (J g^{-1}). Fig. 6 shows the logarithmic conversion rate as function of reciprocal of temperature by this method. In Fig. 6 the steeper slope of the experimental curves versus the iso-conversion lines in the range of $1000/T > 2.70$ is a finite indication of the presence of an auto-catalytically activated initial reaction. The analysis curve in Fig. 7 almost remains constant from the fractional reaction progress 0.1 to 0.9 which indicating a single step reaction.

Here the plot simulates to first-order kinetics. The analysis plot (Fig. 7) extrapolates E and A as function of α. Friedman analysis reveals that the average activation energy of the complex $[Ni(ampy)_2(NO_3)_2]$ is 41 ± 1 kJ mol^{-1} and the corresponding average logarithmic pre-exponential factor (log A (s^{-1})) is 2.54.

3.2.1.2. ASTM method. Kissinger introduced the equation where pre-exponential factor is evaluated on assumption of a first-order reaction [15,16]:

$$\ln \frac{\beta}{T_{j,m}} = -\frac{E}{RT_{j,m}}$$

ASTM E698 method utilizes Kissinger's plot where a reaction of first-order results from the displacement of the maximum temperatures of DSC curves. Kissinger's plot shows a straight line with slope $(-E/R)$ and $T_{j,m}$ is the maximum tem-

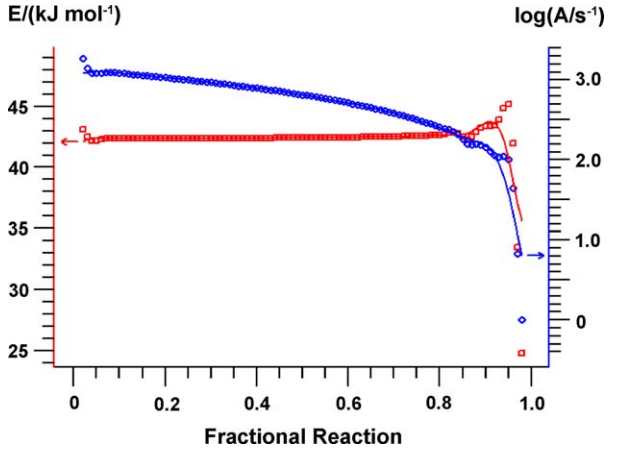

Fig. 7. E and A in Friedman method. Symbols are experimental along with simulated lines.

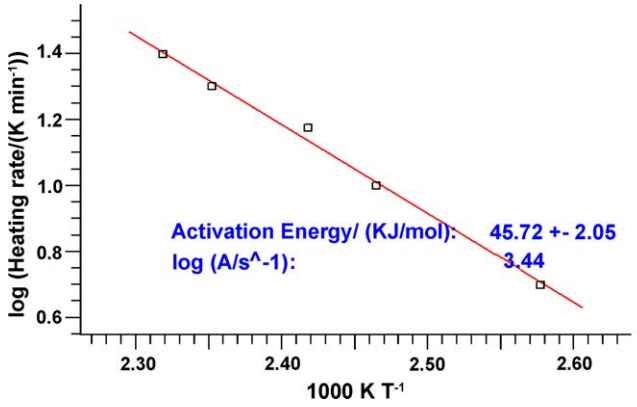

Fig. 8. ASTM plot of $[Ni(ampy)_2(NO_3)_2]$.

perature. The logarithms of heating rates were plotted over the maximum reciprocal temperatures of DSC curves, where the obtained slope gives the activation energy. The pre-exponential factor was obtained on the assumption of a first-order reaction $A = \beta E/RT_{j,m}^2 \exp(E/RT_{j,m})$. $T_{j,m}$ was determined utilizing the smoothed numerical derivatives of dα/dT. The ASTM analysis plot (Fig. 8) of $[Ni(ampy)_2(NO_3)_2]$ shows the activation energy of the complex is $46 \pm 2\,kJ\,mol^{-1}$ and the corresponding average logarithmic pre-exponential factor ($\log A$ (s^{-1})) is 3.44.

3.2.2. Determination of kinetic model of thermal decomposition

Multivariate non-linear-regression (Netzsch TA4 thermokinetics) was applied to determine the most probable kinetic model. The software module Netzsch TA4 thermokinetics numerically solves the relevant differential equations and the parameters of the differential equations are iteratively optimized. Here all the commonly used models were utilized for the determination of activation energy [17–19]. Combination of both iso-conversional and multivariate non-linear-regression can provide most reasonable models than the model-fitting methods. The mentioned models listed in Table 3 are based on correlation coefficient and the "goodness of fit" from a statistical point of view, simulates to a first-order reaction path A → B. The best model imaged from the correlation coefficient is Bna which corresponds to expanded Prout–Tompkins equation $(1-\alpha)^n$ α^a having $F_{exp,}$ F_{crit} 1.00 and 1.09, respectively. Next to this model the others like F*n*, C*n* and F2 fit better. C*n*, which corresponds to the *n*th order reaction with auto catalysis [$f(\alpha)$ in C*n* is $(1-\alpha)^n$ $(1+K_{cat}\alpha)$] through the reactants having $F_{exp,}$ F_{crit} 1.00 and 1.10, respectively. The function $f(\alpha)$ in Bna and C*n* are $(1-\alpha)^{2.08}\alpha^{1.0236E-3}$ and $(1-\alpha)^{2.07}(1+0.0144\alpha)$, respectively. Three-dimensional Jander's diffusion model (D3), the activation energy slightly deviates than the other mentioned models in Table 3, which is very difficult to predict with the similar changes of α with respect to both time and temperature.

3.2.3. Determination of half-life period and rate constant

Based on the predictions of F*n* model, reaction was considered for 25–600 °C. DSC curves calculated within the range of temperature for the decomposition process, this generates the change in concentration of reaction progress. These curves with degree of conversion as a parameter indicates an exponential progress in percentage of conversion with time and temperature. For clarification, thermoanalytical isothermal predictions are investigated in a narrow temperature range 271–320 °C. The conversion shows a maximum at 320 °C. Both the results were taken into account where, the 50% of concentrations changes at 4.85 min, at about 315 °C. Iso-concentration plot dynamic reactants reveal a sigmoidal increase in product concentration to attain a saturation limit at 18.6 min. Rate constant was calculated from the first-order kinetic equation, $k = 0.693/t_{1/2}$. The calculated rate constant and half-life time from iso-concentration plot are $2.381 \times 10^{-3}\,s^{-1}$ and 291 s, respectively.

4. Conclusion

Solid-state kinetics of monoclinic $[Ni(ampy)_2(NO_3)_2]$ complex for thermal release of pyridine, was investigated through both iso-conversional and multivariate non-linear-regression methods. The thermal behavior of $[Ni(ampy)_2(NO_3)_2]$ shows thermal decomposition in three steps with the removal of ligand in an exothermic process. The microscopic surface morphology shows a thread like fiber of NiO calcined at 600 °C. Thermokinetics plays an important role in this magnetically impulsive compound providing the scheme of kinetic process with iterations. The kinetics of elimination of pyridine can be described with a generalized expanded Prout–Tompkins equation. The considerable improvement of the fit quality of DSC data was achieved by single step kinetic model. At the best of our knowledge, the novelty of this work provides the determination of half-life period based on first-order kinetics. The multifariousness application of thermokinetics can be used as a device to

Table 3
Arrhenius parameters in multivariate non-linear-regression methods

Model	E (kJ mol^{-1})	$\log A$ (s^{-1})	Correlation coefficient	n or a or $\log K_{cat}$	F_{exp}	F_{crit} (0.95)
Bna	42.23 ± 0.03	3.12 ± 0.003	0.999998	1.0236E−3 (n = 2.08)	1.00	1.09
An	41.71 ± 0.96	2.73 ± 0.12	0.997951	n = 0.6582	180.5	1.09
C*n*	42.17 ± 0.03	3.11 ± 0.01	0.999998	−1.8412 (n = 2.07)	1.00	1.10
D2	41.82 ± 0.73	2.12 ± 0.09	0.993862		289.4	1.09
D3	47.69 ± 0.68	2.36 ± 0.08	0.996045		207.3	1.09
D4	43.69 ± 0.73	1.75 ± 0.09	0.994710		247.6	1.09
F2	41.12 ± 0.04	2.95 ± 0.01	0.999983		8.58	1.09
F*n*	42.43 ± 0.03	3.14 ± 0.004	0.999998	n = 2.0883	1.18	1.09

present the solid state kinetics a neat through appropriate iterations.

Acknowledgements

I am grateful to Indian Institute of Technology, Guwahati providing the institute fellowship. Special thanks to Mr. G. Padmanabhan providing NETZSCH TA4 software for kinetic analysis.

References

[1] S. Tanase, M. Ferbinteanu, M. Andruh, C. Mathonière, I. Strenger, G. Rombaut, Polyhedron 19 (2000) 1967–1973.
[2] C. Paraschiv, M. Andruh, J–P. Sutter, Inorg. Chim. Acta 351 (2003) 385–388.
[3] S. Bruda, M.M. Turnbull, C.P. Landee, Q. Xu, Inorg. Chim. Acta 359 (2006) 298–308.
[4] L. ORTEP III, J. Farrugia, J. Appl. Crystallogr. 30 (1997) 565.
[5] SMART, SAINT, Siemens Analytical X-ray, Instruments Inc., Madison, WI, 1996.
[6] G.M. Sheldrick, SHELXS-97 and SHELXL-97, University of Göttingen, Göttingen, Germany, 1997.
[7] K. Nakamoto, Infrared and Raman Spectra of Inorganic and Coordination Compounds. Part B, 5th ed., Wiley, New York, 1997.
[8] C. Kittel, Introduction to Solid State Physics, 7th ed., Wiley, New York, 1996.
[9] H.L. Friedman, J. Polym. Lett. 4 (1966) 323–328.
[10] S. Vyazovkin, J. Comput. Chem. 22 (2001) 178–183.
[11] S. Vyazovkin, Int. J. Chem. Kinet. 28 (1996) 95–101.
[12] S. Vyazovkin, Thermochim. Acta 355 (2000) 155–163.
[13] A. Burnham, Thermochim. Acta 355 (2000) 165–170.
[14] M. Maciejewski, Thermochim. Acta 355 (2000) 145–154.
[15] H.E. Kissinger, J. Res. Nat. Bur. Stds. 57 (1956) 217–221.
[16] H.E. Kissinger, Anal. Chem. 29 (1957) 1702–1706.
[17] S. Vyazovkin, C.A. Wight, Thermochim. Acta 340-341 (1999) 53–68.
[18] S. Vyazovkin, J.S. Clawson, C.A. Wight, Chem. Mater. 13 (2001) 960–966.
[19] M.E. Brown, M. Maciejewski, S. Vyazovkin, R. Nomen, J. Sempere, A. Burnham, J. Opfermann, R. Strey, H.L. Anderson, A. Kemmler, R. Keuleers, J. Janssens, H.O. Desseyn, C.-R. Li, T.B. Tang, B. Roduit, J. Malek, T. Mitsuhashi, Thermochim. Acta 355 (2000) 125–143.